A novel high resolution ion wide angle spectrometer

D. Jung, R. Hörlein, D. C. Gautier, S. Letzring, D. Kiefer et al.

Additional information on Rev. Sci. Instrum.

A novel high resolution ion wide angle spectrometer

D. Jung,[1,2,3,a)] R. Hörlein,[3] D. C. Gautier,[1] S. Letzring,[1] D. Kiefer,[2,3] K. Allinger,[2]
B. J. Albright,[1] R. Shah,[1] S. Palaniyappan,[1] L. Yin,[1] J. C. Fernández,[1] D. Habs,[2,3]
and B. M. Hegelich[1,2]

[1]*Los Alamos National Laboratory, Los Alamos, New Mexico 87545, USA*
[2]*Department für Physik, Ludwig-Maximilians-Universität München, D-85748 Garching, Germany*
[3]*Max-Planck-Institut für Quantenoptik, D-85748 Garching, Germany*

A novel ion wide angle spectrometer (iWASP) has been developed, which is capable of measuring angularly resolved energy distributions of protons and a second ion species, such as carbon C^{6+}, simultaneously. The energy resolution for protons and carbon ions is better than 10% at $\sim$50 MeV/nucleon and thus suitable for the study of novel laser-ion acceleration schemes aiming for ultrahigh particle energies. A wedged magnet design enables an acceptance angle of $30°(\sim$524 mrad) and high angular accuracy in the μrad range. First, results obtained at the LANL Trident laser facility are presented demonstrating high energy and angular resolution of this novel iWASP. © *2011 American Institute of Physics*. [doi:10.1063/1.3575581]

I. INTRODUCTION

In the last decade, laser-ion acceleration (LIA) has been studied intensively in order to exploit the unique accelerating gradients setup by ultraintense lasers in plasmas, which are today already 6 orders of magnitude higher than in conventional accelerators. To establish an alternative ion source superior to rf-accelerators in terms of size, costs, and particle beam properties, extensive research has been done in the target normal sheath acceleration regime (TNSA);[1] yet particle energies and conversion efficiencies obtained with TNSA are not suitable for most applications, such as ion fast ignition[2,3] or hadron cancer therapy.[4] Recently, numerous new acceleration mechanisms have been proposed within the radiation pressure (RP) regime, covering radiation pressure acceleration (e.g., light sail[5] and laser piston acceleration[6]) and the break-out-afterburner[7,8] acceleration. While TNSA by virtue of its dynamics predominantly accelerates protons, unless target cleaning is implemented,[9,10] these novel mechanisms enable easy acceleration of heavier ions such as carbon C^{6+}. In particular, critical beam properties such as high-energy cutoffs, angular ion distribution, and conversion efficiencies from laser into particle energy have been shown to be quite different from TNSA in many particle in cell (PIC) experiments.[7,11–13] Here, we present a novel ion wide angle spectrometer (iWASP) suitable for measuring and comparing angular particle beam characteristics of the different acceleration mechanisms experimentally. Traditionally, in TNSA stacks of radiochromic film (RCF) (Refs. 14–16) are used to measure the energy and angular distribution of protons. However, heavier ions such as C^{6+} are stopped within the first few layers of the RCF stack due to their much larger cross section and are thus indistinguishable from the protons, making this method unsuitable for LIA experiments in the new acceleration regimes. Furthermore, conversion efficiency measurements for carbon ions are often done by extrapolating the ion

signal from Thomson parabola (TP; Refs. 17–19) traces and are at best a crude approximation as they usually cover only a very small solid angle (10^{-4} to 10^{-5} msr). The new wide angle spectrometer presented here covers solid angles on the order of 10^{-1} msr and also offers ultrahigh angular resolution with energy resolution of better than 10% at 50 MeV/nucleon carbon C^{6+}, in contrast to the imaging proton spectrometer for very low proton energies of <5 MeV presented in Ref. 20. Hence, the iWASP for the first time enables high accuracy estimates of conversion efficiencies from laser into particle energy and angularly resolved energy distribution measurements of proton as well as carbon ions, as compared with extrapolation from Thomson parabola traces or RCF stacks.

II. SPECTROMETER DESIGN AND BENCHMARKING

The ion wide angle spectrometer is based on a magnetic field perpendicular to the ion propagation direction and introduces an energy dependent dispersion of the particle beam. A long slit is positioned parallel to and in front of the magnetic field [see Fig. 1(a)]. The data obtained from the iWASP thus show the energy distribution of the source ions angularly resolved in the dimension along the slit, allowing for detailed comparison of results obtained from PIC simulations and experiments. First experiments within the RP regime have already shown proton and carbon ion energies exceeding tens of MeV/nucleon.[19,22–24] The energy resolution of the iWASP, which is strongly coupled to its acceptance angle, should be at least 10% at these particles energies. To maximize energy resolution and acceptance angle simultaneously, a strong magnetic field with a large gap between the magnets is required. To overcome these conflicting requirements, a wedged yoke design has been implemented, trading field homogeneity for field strength. To calculate the resulting particle traces through the spectrometer and to estimate the energy resolution, a simplified Lorentz equation with zero electric field can

---

a)Electronic mail: daniel.jung@physik.uni-muenchen.de.
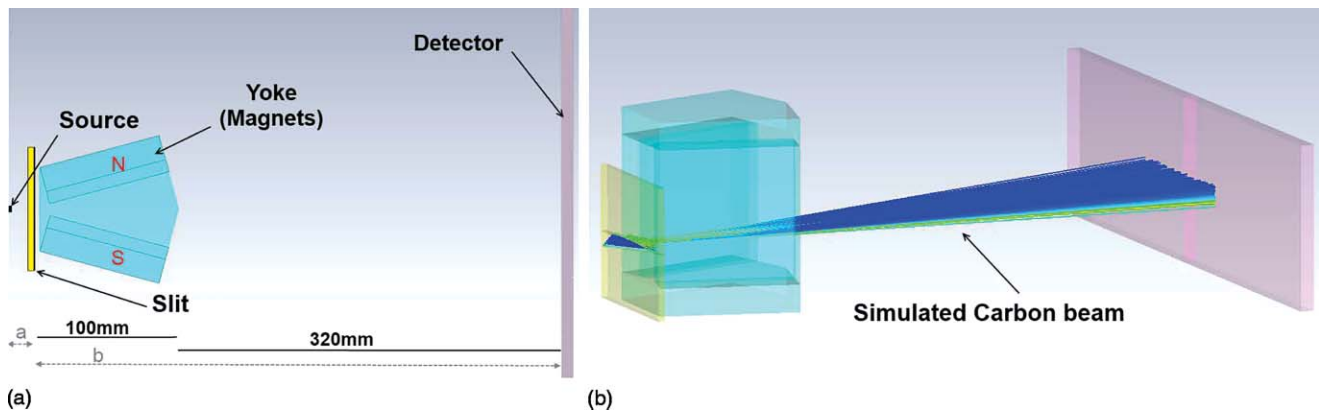
82, 043301-1

FIG. 1. (Color online) (a) Top view of the iWASP, with from left to right, the source, the slit, the yoke, and the detector. (b) Side view showing a simulated trace of carbon C^{6+} ions calculated with CST.[21]

be used

$$\frac{d\vec{p}}{dt} = q\left(\frac{\vec{p}}{m\gamma} \times \vec{B}\right), \tag{1}$$

where m, q, and $\vec{B}$ are the ion mass, charge, and magnetic field, respectively. Time is measured in the laboratory frame with $\vec{p}$ the relativistic momentum and γ the Lorentz factor. A more detailed analysis can be found in Ref. 19. The spectrometer presented here was designed for an acceptance angle of 30° and particle energies on the order of 50 MeV/nucleon. Thus, the wedge half-angle is 15°, where the gap between the two NdFeB magnets is 10 mm at the front and 62 mm at the far end. In order to match the usable magnetic field with a particle cone of 30°, it has to be placed at a distance of about 20 mm from the target (particle source). Here, the energy resolution for a specific charge to mass ratio depends on the drift length, the magnetic field and the source magnification. In particular, the slit in front of the magnets introduces a pinhole-camera-like magnification of the source on the detector in the dimension perpendicular to the slit. The magnification depends on the ratio of a to b, which are the distances from the slit to the particle source and to the detector, respectively. An approximate formula for the energy resolution $\Delta E_{kin}/E_{kin}$ of the iWASP can be obtained by solving the reduced Lorentz equation in the nonrelativistic case and calculating the resulting source magnification on the detector plane

$$\frac{\Delta E_{kin}}{E_{kin}} = \frac{2s}{y(1-(s/2y)^2)^2} \approx \frac{2s}{y}, \tag{2}$$

where y is $(qBl_B(D+0.5l_B))/(2mE_{kin})^{0.5}$ with l_B the length of the magnetic field (along propagation direction) and D the drift from the end of the field to the detector. Here, $s = d + b/a(d + x)$ is the image of the source on the detector with d the slit width and x the source size, assuming an incoherent particle emission. To maintain a sufficiently high energy resolution for the setup presented here, the width of the slit must not be bigger than a few tens of micrometers. The angular accuracy of the spectrometer can be derived from a careful trigonometric consideration, assuming an angularly incoherent particle emission. The lower limit of the angular error $\Delta\alpha$, i.e., the positive and negative deviation of a given angle α is

$$\Delta\alpha = \tan^{-1}\left(\tan(\alpha) \pm \frac{x_{s,d}}{2(a+b)}\right), \tag{3}$$

where $x_{s,d}$ is the greater of either the source size or the detector pixel size. It should be noted that for some detectors such as the image plate (IP), the angular error might be increased by ions passing through two or more pixels of the detector due to their oblique incidence. This effect can be reduced by a curved detector plane. While this gives the angular error for a single ion, the binning of the data (to extract a complete energy spectrum) will dominate the final angular uncertainty (set $x_{s,d}$ as the binning size), resulting in uncertainties below 100 μmrad for the parameters presented here. Although the iWASP lacks the charge to mass separation of a Thomson parabola, it is still suitable for many LIA experiments where two species with significantly different mass are accelerated; e.g., from proton–carbon targets (or similar proton–ion targets such as diamond, diamondlike carbon or CH_x foils. Here, a stacked detector can be used to distinguish between the two species by their different stopping powers. The spectrometer presented here includes a stacked detector consisting of a CR39 nuclear track detector[25] for the carbon ions, followed by an IP (Ref. 26) to detect protons. The CR39 allows for suppression of the proton signal by using a short etching time, so that only pits of heavier ions, here the carbon ions, will become visible, while the pit size of protons stays below the detection limit.[27] Depending on the CR39 thickness, carbon ions will be stopped within the CR39 up to their breakthrough energy, beyond which the carbon ion energy is high enough to pass the CR39, i.e., the Bragg peak is not within the CR39 anymore. For the same thickness the breakthrough energy of protons is significantly lower;[28] the proton signal can thus be recorded on the image plate without being overlapped by carbon ions, provided the protons with the highest energy are deflected less than carbon ions exceeding the breakthrough energy (see Fig. 2). In an advanced setup of the iWASP, charge to mass separation capability could be added for selected angles; here, vertical slits in the detector can be used to transport the ion beam behind the detector through pairs of electrodes to introduce charge to mass separation within the electric fields.
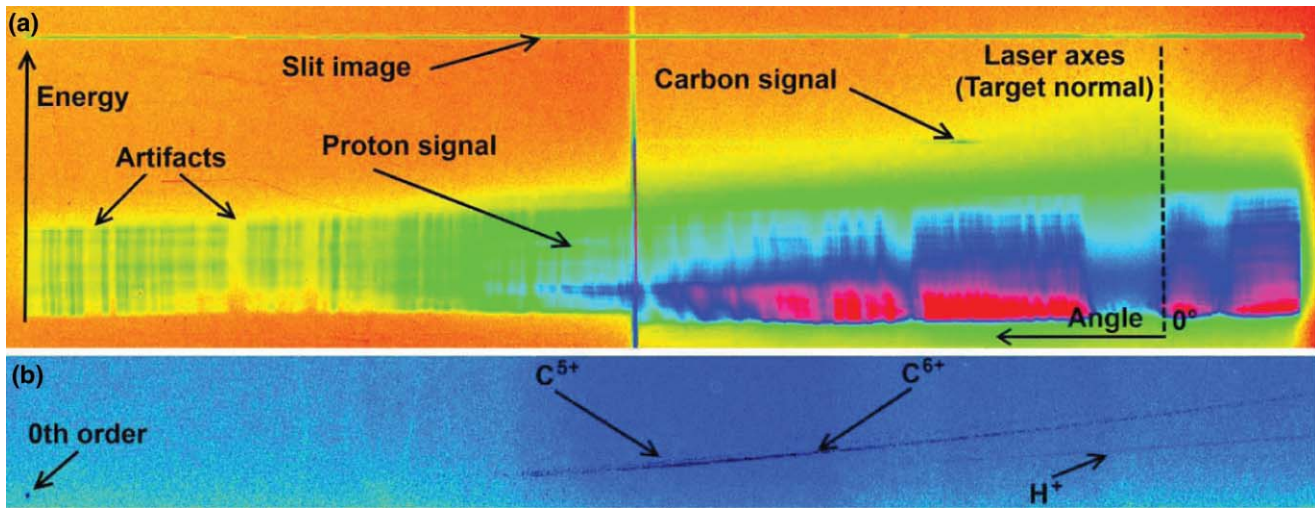
FIG. 2. (Color online) (a) iWASP data recorded on the IP from a 1 μm target (normal incidence) showing the image of the slit on the top, a faint line of carbon ions beyond the breakthrough energy (see text) and the proton signal starting at the bottom of the IP at their low energy cutoff of about 11 MeV; color shows particle density in arbitrary units. Note, that vertical features in the data are a result of nonuniformities in the 20 μm slit aperture. The thick vertical line in the middle is a result of two pieces of CR39 intersecting in front of the IP; slightly different thicknesses in the CR39 also result in an asymmetry of the low-energy cutoff line visible here. (b) Data recorded on a Thomson parabola from a 1 μm solid diamond target showing a proton and a dominant carbon C^{6+} signal among a very faint carbon C^{5+} line.

Next, we present first results from a campaign performed at the Trident laser facility[29,30] showing excellent performance of the iWASP. The spectrometer has been used to probe an ion beam accelerated by an 80 J, 550 fs pulse at a wavelength of 1054 nm (160 TW). The beam is focused down to a spot diameter of 6 μm (first Airy minimum) with an F/3 off-axis parabolic mirror resulting in on-target intensity of $\sim 2 \times 10^{20}$ W/cm^2. Free-standing ultrathin diamondlike carbon foils with submicron thickness are illuminated at normal incidence to provide a beam of protons and predominantly carbon C^{6+} ions of up to about 50 and 40 MeV/nucleon, respectively. A slit made of 10 mm thick solid copper with a slit width of approximately 20 μm has been placed directly in front of the yoke. Due to setup constraints, the slit's distance to the target was 25 mm (instead of 20 mm) resulting in an acceptance angle of about 20°. A drift of 320 mm to the detector measured from the end of the yoke yields an angular uncertainty of $\ll$100 μrad (along iWASP center) and a resolution of 5% for protons and 8% for carbon C^{6+} at energies of 50 and 40 MeV/nucleon, respectively; the source image size $s = (350 \pm 50)\,\mu$m has been extracted from the IP data and the average magnetic field has been measured to be about 440 mT [see Fig. 2 and Eq. (2)]. In this specific setup, the solid angle captured by the iWASP is $\sim$0.25 msr. This is 3 orders of magnitude larger than in standard TP configurations with typical solid angles on the order of 10^{-5} msr and significantly increases accuracy and validity of conversion efficiency estimates of laser to particle energy. The detector used in this experiment consists of a 1 mm thick CR39 in front of a standard BAS-TR IP (no protective layer, active phosphor layer $\sim$50 μm); a layer of 30 μm Al has been added in front of the CR39 to reduce the flux on the CR39 and to protect the IP from direct laser light penetrating the slit and scattered laser light. With this setup the CR39 can record carbon C^{6+} from $\sim$30 MeV to energies far beyond their breakthrough en-

ergy of $\sim$230 MeV, where the deposited energy in the CR39 is still high enough to generate visible pits (also on the backside of the CR39); the IP measures protons above 11 MeV and accordingly carbon C^{6+} above 230 MeV. In Fig. 2(a) the particle signal from a 1 μm solid diamond target with normal laser incidence recorded on the IP positioned behind the CR39 is shown. Here, the image of the slit aperture can be seen on the top, followed by a faint signal of carbon ions with energies above 230 MeV, i.e., beyond their breakthrough energy for the CR39; below follows the proton signal starting at the bottom of the IP at about 11 MeV. Note that energy increases from the bottom of Fig. 2(a) toward the slit image. The carbon data recorded on the CR39 extracted after 30 min of etching at 80 °C show a very similar distribution for the carbon C^{6+} ions [see Fig. 3(b)]; contamination of the carbon C^{6+} data by other species such as oxygen and nitrogen is expected to be insignificant and should be negligible for other charge states of carbon, as seen on TP data from the same and also previous experiments using the same laser intensities and targets. In Fig. 2(b) TP data obtained from a 1 μm thick solid diamond target during the same campaign is shown; here the predominant species is C^{6+} with only a very faint contribution of C^{5+} and no other species than protons. A more accurate estimate of the contamination will be obtained in future experiments using the extended setup of the iWASP, as explained before, where the species contribution can be measured on the same shot. Figure 3(a) shows the proton spectrum extracted from the raw data shown in Figs. 2(a) and 3(b) the carbon C^{6+} spectrum extracted from the CR39 of the corresponding shot. The low energy cutoff lines from the carbon ion and proton signals [see Fig. 2(a)] have been used to extrapolate the average magnetic field versus angle for extraction of the energy spectrum. For the 1 μm diamond target used here, the TNSA acceleration mechanism is expected to be dominant. In fact, a well beamed proton and

ticle beams. With the extended version of the iWASP, containing additional electrodes for charge to mass separation, one can not only obtain accurate information on the different species accelerated, but also retrieve information on angular ion distributions with high accuracy.
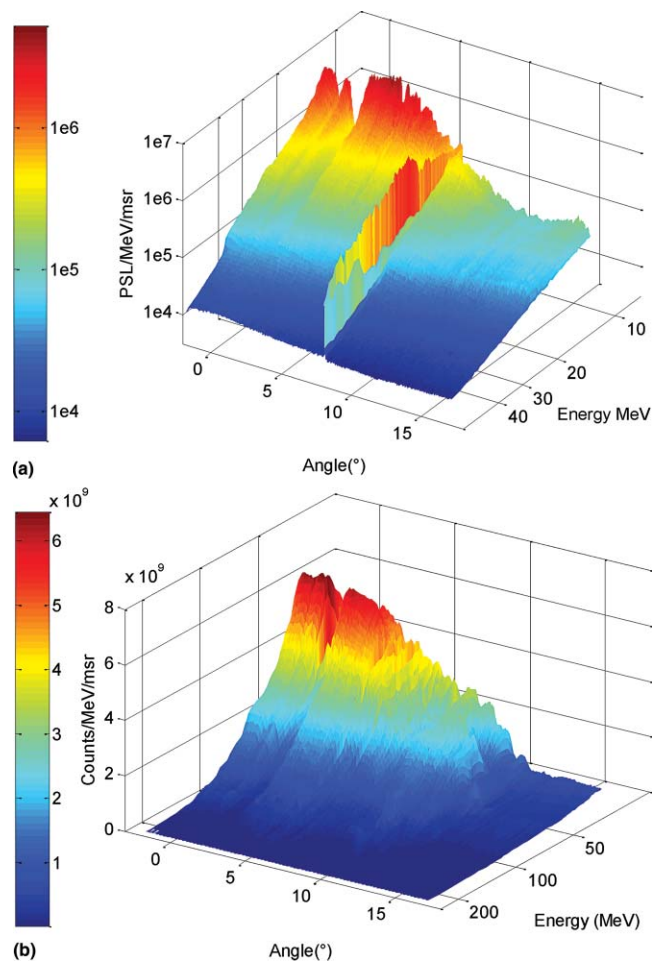

FIG. 3. (Color online) (a) Proton spectrum extracted from the IP data shown in Fig. 2 and (b) carbon C^{6+} spectrum extracted from the CR39 of the corresponding shot; the spectra show ion distributions peaking target normal at $0°$ typical for TNSA dominated LIA.

carbon ion signal with the highest energies and particle numbers around the target normal at $0°$ is visible; both the high energy cutoffs and particle numbers drop with increasing angle agreeing well with the TNSA model. A more detailed analysis, including conversion efficiency estimates and ion beam profile changes will be shown in a dedicated publication.

III. CONCLUSIONS

We presented a novel iWASP and first experimental results showing proton and carbon ion angular distribution at the same time, by use of a stacked detector system. The iWASP will be a helpful tool for future investigation of conversion efficiencies and beam distribution measurements of laser accelerated ions; this is especially so, when dealing with ion beams composed of multiple ion species and charge states, where a standard RCF stack is not suitable to measure beam distributions anymore. Several acceleration mechanisms have been proposed within the RP regime, some of which yield monoenergetic ion spectra,[23] where the iWASP will give significantly more information and accuracy on the beam properties as compared to measurements with a standard TP, thus increasing validity of experimental data on monoenergetic par-

[1] S. P. Hatchett, C. G. Brown, T. E. Cowan, E. A. Henry, J. S. Johnson, M. H. Key, J. A. Koch, A. B. Langdon, B. F. Lasinski, R. W. Lee, A. J. Mackinnon, D. M. Pennington, M. D. Perry, T. W. Phillips, M.Roth, T. C. Sangster, M. S. Singh, R. A. Snavely, M. A. Stoyer, S. C. Wilks, and K.Yasuike, in *Proceedings of the 41st Annual Meeting of the Division of Plasma Physics of the American Physical Society, Seattle, WA, 1999* [Am. Phys. Soc. **7**, 2076 (2000)].

[2] M. Roth, T. E. Cowan, M. H. Key, S. P. Hatchett, C. Brown, W. Fountain, J. Johnson, D. M. Pennington, R. A. Snavely, S. C. Wilks, K. Yasuike, H. Ruhl, F. Pegoraro, S. V. Bulanov, E. M. Campbell, M. D. Perry, and H. Powell, Phys. Rev. Lett. **86**, 436 (2001).

[3] J. C. Fernández, B. J. Albright, K. A. Flippo, B. M. Hegelich, T. J. Kwan, M. J. Schmitt, and L. Yin, J. Phys.: Conf. Ser. **112**, 022051 (2008).

[4] T. Tajima, D. Habs, and X. Yan, Rev. Accel. Sci. Tech. **2**, 201 (2009).

[5] B. Qiao, M. Zepf, M. Borghesi, and M. Geissler, Phys. Rev. Lett. **102**, 145002 (2009).

[6] T. Esirkepov, M. Borghesi, S. V. Bulanov, G. Mourou, and T. Tajima, Phys. Rev. Lett. **92**, 175003 (2004).

[7] L. Yin, B. J. Albright, B. M. Hegelich, K. J. Bowers, K. A. Flippo, T. J. T. Kwan, and J. C. Fernandez, Phys. Plasmas **14**, 056706 (2007).

[8] B. J. Albright, L. Yin, K. J. Bowers, B. M. Hegelich, K. A. Flippo, T. J. T. Kwan, and J. C. Fernandez, Phys. Plasmas **14**, 094502 (2007).

[9] M. Hegelich, S. Karsch, G. Pretzler, D. Habs, K. Witte, W. Guenther, M. Allen, A. Blazevic, J. Fuchs, J. C. Gauthier, M. Geissel, P. Audebert, T. Cowan, and M. Roth, Phys. Rev. Lett. **89**, 085002 (2002).

[10] B. M. Hegelich, B. Albright, P. Audebert, A. Blazevic, E. Brambrink, J. Cobble, T. Cowan, J. Fuchs, J. C. Gauthier, C. Gautier, M. Geissel, D. Habs, R. Johnson, S. Karsch, A. Kemp, S. Letzring, M. Roth, U. Schramm, J. Schreiber, K. J. Witte, and J. C. Fernandez, Phys. Plasmas **12**, 056314 (2005).

[11] X. Q. Yan, C. Lin, Z. M. Sheng, Z. Y. Guo, B. C. Liu, Y. R. Lu, J. X. Fang, and J. E. Chen, Phys. Rev. Lett. **100**, 135003 (2008).

[12] O. Klimo, J. Psikal, J. Limpouch, and V. T. Tikhonchuk, Phys. Rev. ST Accel. Beams **11**, 031301 (2008).

[13] A. Macchi, S. Veghini, and F. Pegoraro, Phys. Rev. Lett. **103**, 085003 (2009).

[14] W. McLaughlin, J. Puhl, M. Al-Sheikhly, C. Christou, A. Miller, A. Kovács, L. Wojnarovits, and D. Lewis, Radiat. Prot. Dosim. **66**, 263 (1996).

[15] R. Clarke, P. Simpson, S. Kar, J. Green, C. Bellei, D. Carroll, B. Dromey, S. Kneip, K. Markey, P. McKenna, W. Murphy, S. Nagel, L. Willingale, and M. Zepf, Nucl. Instrum. Methods Phys. Res. A **585**, 117 (2008).

[16] F. Nurnberg, M. Schollmeier, E. Brambrink, A. Blazevic, D. C. Carroll, K. Flippo, D. C. Gautier, M. Geissel, K. Harres, B. M. Hegelich, O. Lundh, K. Markey, P. McKenna, D. Neely, J. Schreiber, and M. Roth, Rev Sci. Instrum. **80**, 033301 (2009).

[17] J. J. Thomson, Philos. Mag., Ser. 6 **22**, 469 (1911).

[18] K. Harres, M. Schollmeier, E. Brambrink, P. Audebert, A. Blazevic, K. Flippo, D. C. Gautier, M. Geissel, B. M. Hegelich, F. Nurnberg, J. Schreiber, H. Wahl, and M. Roth, Rev. Sci. Instrum. **79**, 093306 (2008).

[19] D. Jung, R. Horlein, D. Kiefer, S. Letzring, D. C. Gautier, U. Schramm, C. Hubsch, R. Ohm, B. J. Albright, J. C. Fernandez, D. Habs, and B. M. Hegelich, Rev. Sci. Instrum. **82**, 013306 (2011).

[20] H. Chen, A. U. Hazi, R. van Maren, S. N. Chen, J. Fuchs, M. Gauthier, S. L. Pape, J. R. Rygg, and R. Shepherd, Rev. Sci. Instrum. **81**, 10D314 (2010).

[21] See http://www.cst.com for CST AG, "CST Particle Studio 2010."

[22] A. Henig, D. Kiefer, K. Markey, D. C. Gautier, K. A. Flippo, S. Letzring, R. P. Johnson, T. Shimada, L. Yin, B. J. Albright, K. J. Bowers, J. C. Fernández, S. G. Rykovanov, H.-C. Wu, M. Zepf, D. Jung, V. K. Liechtenstein, J. Schreiber, D. Habs, and B. M. Hegelich, Phys. Rev. Lett. **103**, 045002 (2009).

[23] A. Henig, S. Steinke, M. Schnürer, T. Sokollik, R. Hörlein, D. Kiefer, D. Jung, J. Schreiber, B. M. Hegelich, X. Q. Yan, J. Meyer-ter Vehn, T. Tajima, P. V. Nickles, W. Sandner, and D. Habs, Phys. Rev. Lett. **103**, 245003 (2009).

[24] S. Steinke, A. Henig, M. Schnürer, T. Sokollik, P. Nickles, D. Jung, D. Kiefer, R. Hörlein, J. Schreiber, T. Tajima, X. Yan, M. Hegelich, J. Meyer-ter Vehn, W. Sandner, and D. Habs, Laser Part. Beams **28**, 215 (2010).

[25] R. L. Fleischer, P. B. Price, and R. M. Walker, J. Appl. Phys. **36**, 3645 (1965).

[26] I. J. Paterson, R. J. Clarke, N. C. Woolsey, and G. Gregori, Meas. Sci. Technol. **19**, 095301 (2008).

[27] Y. Rao, A. Davis, T. Spencer, and R. Filz, Nucl. Instrum. Methods **180**, 153 (1981).

[28] J. F. Ziegler, J. P. Biersack, and U. Littmark, *The Stopping and Range of Ions in Solids* (Pergamon, New York 1985), Vol. 1.

[29] J. Workman, J. Cobble, K. Flippo, D. C. Gautier, and S. Letzring, Rev. Sci. Instrum. **79**, 10E905 (2008).

[30] R. C. Shah, R. P. Johnson, T. Shimada, K. A. Flippo, J. C. Fernandez, and B. M. Hegelich, Opt. Lett. **34**, 2273 (2009).